RESEARCH ARTICLE

Dynamic Programming for Thermal Management of Automotive Fuel Cell Systems: Investigating Hydrogen Saving Potential

PIER GIUSEPPE ANSELMA[1,2], **(Member, IEEE), SARA LUCIANI**[1,2], **(Member, IEEE), AND ANDREA TONOLI**[1]

[1]Department of Mechanical and Aerospace Engineering (DIMEAS), Politecnico di Torino, 10129 Turin, Italy
[2]Center for Automotive Research and Sustainable Mobility (CARS), Politecnico di Torino, 10129 Turin, Italy

Corresponding author: Sara Luciani (sara.luciani@polito.it)

ABSTRACT Thermal management strategies implemented on-board fuel cell electrified vehicles (FCEVs) are currently based on heuristic reactive approaches. In this framework, developing predictive thermal management approaches that anticipate the travel needs of FCEV users could lead to improved hydrogen savings. However, the theoretical hydrogen saving achievable by predictive thermal management needs assessment first to quantify the technical and economical viability of the technology proposal. This paper lays the foundations in this domain by analyzing the a priori optimal thermal management of a fuel cell system in an FCEV. Initially, an electrochemical and thermal modeling technique for the fuel cell system is described. A reactive rule-based approach is then selected as the baseline controller for the coolant rate and the instantaneous radiator fan state of the FCEV. Then, the optimal control problem formulation for the thermal management of fuel cell systems in FCEVs is discussed and solved using a dynamic programming (DP) based optimization approach that makes use of a priori information about the entire driving mission. The fuel cell system is evaluated while the FCEV performs one to ten repetitions of the Worldwide Harmonized Light Vehicle Test Cycle (WLTC) at different ambient temperatures ranging from −20 °C to 40 °C. When compared to the baseline reactive control technique, the offline optimal benchmark can save up to 10.2% hydrogen. Results presented in this paper demonstrate the potential of hydrogen saving achievable by improving the thermal management of automotive fuel cell systems. Moreover, they may be used to develop and benchmark real-time capable predictive thermal management strategies for fuel cell systems in FCEVs.

INDEX TERMS Dynamic programming, electrified vehicle, fuel cell system, hydrogen economy, optimal control, thermal management.

I. INTRODUCTION

Several uncertainties in fuel cost and supply, as well as air pollution, currently pose substantial challenges to the automobile industry [1], [2], [3]. To address these concerns, several researchers and car makers began researching and improving pure electric vehicles and fuel cell electrified vehicles (FCEV). FCEVs are particularly promising since

they do not produce tailpipe emissions, they feature extended driving ranges, they can be refilled quickly, and they have good overall energy efficiency [4], [5], [6]. The temperature of a fuel cell system impacts for example the fuel cell stack humidity, power output capabilities, voltage, leakage current, catalyst tolerance, and durability [7], [8], [9]. As a result, a robust thermal management system is essential to ensure the performance and temperature stability of a fuel cell system while minimizing the electric power consumption of the auxiliary components [10], [11], [12]. In the following up of this

The associate editor coordinating the review of this manuscript and approving it for publication was Lei Wang.

section, research works from the literature related to thermal management of FCEVs are reviewed first and the research gaps are pointed out. Subsequently, the contributions of the present study are highlighted.

A. LITERATURE REVIEW ON THERMAL MANAGEMENT OF FCEVs

Many of the control strategies for thermal management of fuel cell systems described in the literature are of reactive type [13], [14], [15], [16]. They are primarily concerned with the operational stack temperature without taking into account the efficiency of the auxiliary systems in the thermal loop. On/off switching controllers and PID (proportional integral derivative) controllers have been widely used in various automotive thermal control applications due to their dependability and inexpensive cost [17], [18]. For example, a PID controller is used to set a positive temperature coefficient for an electric heater that preheats the fuel cell stack by heating the coolant in [19]. A fuzzy-based temperature controller for electric car cabin heating is suggested in [20]. Under various start circumstances, the control was able to maintain the desired temperature. On the other hand, a fuzzy incremental PID strategy to control the temperature of a proton exchange membrane (PEM) fuel cell is presented in [21]. A self-learning intelligent control approach for assuring cabin thermal comfort is discussed in [22], while multiple control algorithms to adjust the PEM fuel cell stack temperature to the reference value under transient settings are examined in [23].

Predictive thermal management techniques recently started gaining attention as an alternative to state-of-the-art reactive controllers in the domain of electrified vehicles [24], [25]. They exploit forecasts of future operating conditions (e.g. based on traffic or road information) to minimize the FCEV hydrogen consumption and to enhance the overall efficiency of the fuel cell stack. For example, a feedback controller with model reference adaptive control to adjust the coolant intake temperature was recently developed by [23]. Furthermore, a model predictive control (MPC) technique to regulate the blowers in the fuel cell system was suggested in [26]. MPC can also manage water or H2 excess ratio in PEM fuel cell to improve the performances and efficiency of the fuel cell system itself, as demonstrated in [27] and in [28], respectively. Nonetheless, the generated predictive controllers were not benchmarked against the relevant global best solution, and the studies only took into account a subset of the thermal loop of a PEM fuel cell system for automotive applications. In general, in the reviewed literature, a systematic method to assess the potential of predictive thermal management for FCEVs in terms of the optimal operation of the fuel cell system (including the auxiliary components for thermal management) still needs substantial development. This is particularly true when considering demanding vehicle use scenarios, such as when encountering extreme ambient temperatures and long-distance journeys for example. Limited contributions have already been done by the authors in this

framework, yet much work is still required when it comes to assess different temperature and driving conditions [29], [30].

B. CONTRIBUTION OF THE PRESENT STUDY

The previous sub-section highlighted how on one hand current thermal control strategies for the fuel cell system are of reactive type, while on the other hand currently available predictive thermal management approaches regulate single parameters or components of the fuel cell system only (e.g. coolant intake, temperature blower). Predictive thermal management approaches could regulate the entire fuel cell system of FCEVs by anticipating the travel needs of the vehicle users, however this requires first an assessment of the theoretical efficiency improvement and hydrogen saving achievable by developing such technology. From the research works reviewed above, it has emerged how such analysis is currently missing in the literature. To contribute filling the highlighted research gap, this paper aims at assessing the potential of hydrogen saving achievable through off-line optimal control of fuel cell systems in FCEVs. Three primary goals are targeted here to contribute addressing the stated research gap:

1) Identifying optimal working modes for the thermal management of fuel cell systems in FCEVs by controlling at each time instant the radiator fan state and the coolant mass flow rate provided by the thermal pump.
2) Establishing a reference and a benchmark for the development of real-time capable predictive control techniques for thermal management of fuel cell systems in FCEVs.
3) Performing a sensitivity analysis of the hydrogen saving capability predicted by the implemented optimal control approach compared with a baseline reactive control strategy in different operating conditions for the FCEV, e.g. extreme ambient temperatures and variable driving lengths.

The following is how this paper is structured. Section II describes the fuel cell electrochemical and thermal models under consideration. Section III proposes a formulation of the optimal control problem for the thermal management of fuel cell systems in FCEVs. Finding the global optimal solution for the illustrated control problem is described by implementing dynamic programming (DP). The baseline reactive control strategy is illustrated along. Section IV evaluates the capability of the optimal control solution as a hydrogen saving enabler by simulating the FCEV in driving missions at different ambient temperatures and by varying the length of the performed driving mission. Conclusions are finally outlined in Section V.

II. FUEL CELL SYSTEM MODELING

This section illustrates the numerical model of the fuel cell system both from electrochemical and thermal points of view. In this work, the numerical method used to model the fuel cell system is semi-empirical and considers also its

TABLE 1. Representative FCEV parameters.

Component	Parameter	Value
Vehicle	Mass	1500 kg
	Frontal area	2.0 m2
	Drag coefficient	0.335
	Tyre radius	0.282 m
Electric motor	Maximum power	75 kW
Transmission	Direct drive ratio	6.67
Battery pack	Nominal voltage	292 V
	Capacity	7.4 Ah
Fuel cell	Maximum power	55 kW
system	Cell area	678 cm2
	Number of cells	210
	Max cell voltage	0.94 V

transient behaviour. It has been developed by Virginia Tech in collaboration with National Renewable Energy Laboratory (NREL) and implemented in the Advisor™ 2003 simulation tool embedded in Matlab�® software [31]. Moreover, its performance was evaluated experimentally by comparing it with the data collected on-board a real vehicle. The fuel cell model is selected as it can be fully integrated into the optimal control strategy for thermal management. However, it may be easily substituted and the approach outlined in the following section remains applicable. Fig. 1 illustrates a schematic diagram of the selected fuel cell system highlighting the interaction between the components of the system. Both electrochemical and thermal behaviors are assessed for the fuel cell stack and the related auxiliary system. Here, all the described numerical models are implemented in MATLAB® software. In the following up of this section, the model inputs will be described first. Then, the electrochemistry model of the fuel cell stack will be detailed. The following part will illustrate the thermal model of the fuel cell stack along with the modelling of the electric power consumption of the auxiliary system components. Finally, the net electrical power provided by the fuel cell system will be evaluated. Data considered in this work for a representative fuel cell electrified passenger car are reported in Table 1 and have been inherited from Advisor™. It should be reminded that the thermal management strategy described in this paper could be applied to any vehicle size and any powertrain sizing layout in terms of battery capacity and fuel cell power, other than to the vehicle model that is representative of the data shown in Table 1.

A. MODEL INPUTS

The profile of the target vehicle speed over time for the selected driving mission is considered as input. The considered FCEV is a passenger car powered by an electric motor that is linked to the wheels through a direct drive. The electric motor can be powered by both the fuel cell system and a battery pack. A vehicle supervisory control algorithm and an FCEV powertrain model are implemented. They allow for managing the instantaneous electrical power split between the fuel cell system and the high-voltage battery pack. Here, the vehicle supervisory control algorithm is a rule-based thermostatic logic inherited from Advisor™ 2003 [32]. In particular,

the fuel cell system is set to be activated in case either the battery pack cannot provide the requested power alone, or the battery state-of-charge (SOC) is below a lower limit (set as 40% here), or the average power request in the precedent 5 seconds is higher than a threshold which is set around 9kW here. Once activated, the fuel cell system is set to be on until either the instantaneous power request falls below a lower threshold (set as 7.7kW here), or the battery SOC is above an upper limit (set as 80% here). When the fuel cell system is in operation, the value of its controlled power is set according to the battery SOC. The lower the value of SOC, the higher the power request to the fuel cell system. The FCEV is simulated performing the Worldwide Harmonized Light Vehicle Test Cycle (WLTC) which involves a 30-minute 23.4 km drive cycle. In this case, the fuel cell system power request obtained by the FCEV supervisory control logic is highlighted in red in Fig. 2. Moving on, this power profile over time will be considered as input to the fuel cell system thermal model. Other than the net fuel cell system power request ($P_{system-request}$), the vehicle speed is also received as input by the fuel cell system model. This latter is organized in two main sub-models which respectively account for electrochemical and thermal phenomena.

B. ELECTROCHEMISTRY MODEL

The electrochemistry model allows for fulfilling two main purposes as regards assessing the operating conditions of the fuel cell system:

1) Determine the system electrical operating conditions in terms of voltage and current density along with the H2 mass flow rate;
2) Evaluate the heat generated by the system, which is in turn fed to the thermal model.

In this framework, an iterative solver needs implementation to make sure that the net electric power generated by the fuel cell system balances the corresponding vehicle power request. An initial guess is required for the stack current density I_{stack}. Then, the cell voltage V_{cell} can be determined using the polarization equation developed by Nelson and reported in (1):

$$
\begin{aligned}
V_{cell}(I_{stack}, T_{stack}, p_{O2}) = {} & OCV_{cell} - V_{tafel}(I_{stack}) \\
& - V_{ohmic}(I_{stack}, T_{stack}) \\
& - V_{concentration}(I_{stack}, p_{O2}) \\
& + V_{temperature}(I_{stack}, T_{stack}) \quad (1)
\end{aligned}
$$

where OCV_{cell} and V_{tafel} are the cell open-circuit voltage and a term related with activation voltage loss as a function of the stack current density. V_{ohmic} stands for a voltage drop term related to resistance or ohmic losses in the cell as a function of the stack current density and temperature T_{stack} in kelvin as provided by the thermal model. $V_{concentration}$ accounts for the concentration of mass transportation losses in the cell as a function of the stack current density and the oxygen partial pressure at the cathode inlet p_{O2}. Finally, $V_{temperature}$ considers the effects of the stack temperature on the cell
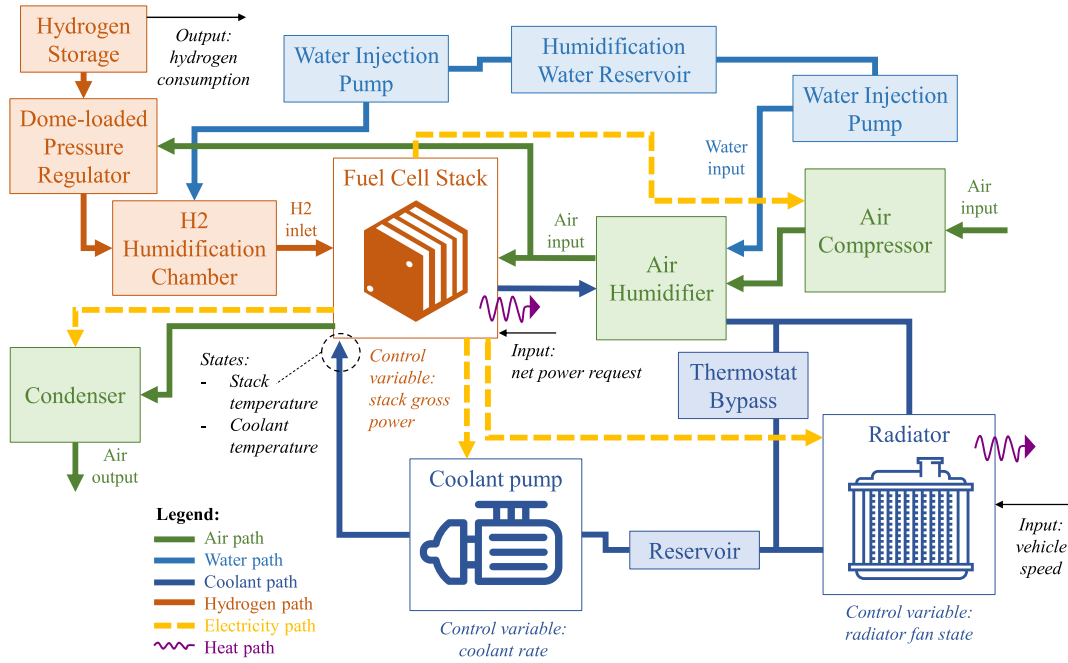
FIGURE 1. Schematic diagram of the fuel cell system including fuel cell stack and auxiliary system.
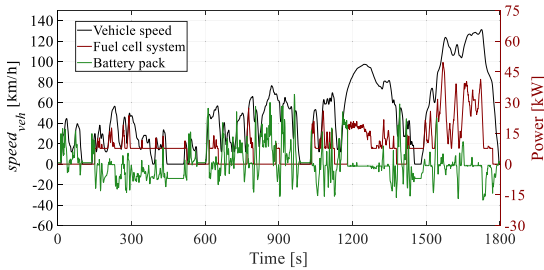

FIGURE 2. Time series of the net electric power requests for the fuel cell system and the battery pack in WLTC according to the FCEV supervisory control logic.

voltage. The gross fuel cell system power $P_{stack-gross}$ in watts can then be obtained using (2):

$$P_{stack-gross} = j_{stack} \cdot V_{cell} \cdot A_{cell} \cdot n_{cell} + P_{aux} \quad (2)$$

where j_{stack} is the stack current density, P_{aux} is the power required by the auxiliary components, A_{cell} and n_{cell} are the area of a single cell in centimetres square and the number of cells contained in the stack, respectively. Once the value of $P_{stack-gross}$ is known, the H2 mass flow rate $\dot{m}_{H2}$ in kilograms per second can be evaluated using (3) [33].

$$\dot{m}_{H2} = \frac{P_{stack-gross} \cdot 1.05e^{-8}}{V_{cell}} \quad (3)$$

which can be derived by (4)

$$\dot{m}_{H2*} = \frac{P_{stack-gross}}{2V_{cell}F} \quad (4)$$

where H2 mass flow rate is in moles per seconds and F is the Faraday constant ($96458 \ C \cdot mol^{-1}$).

Finally, the instantaneous heat generated by the stack (Q_{stack}) can be obtained using (5):

$$Q_{stack} = \dot{m}_{H2} \cdot LHV_{H2} - P_{stack-gross} \quad (5)$$

where LHV_{H2} stands for the hydrogen lower heating value which is assumed being 1.1968e8 J/kg here.

C. THERMAL MODEL OF THE STACK AND AUXILIARY POWER CONSUMPTION

Looking at Fig. 1, modelling the thermal behavior of the fuel cell stack and the electric power consumption of the auxiliary systems involves six main components represented by the air compressor, the coolant pump, the radiator fan, and the condenser fan along with the fuel cell stack and the humidifier. In general, the thermal model receives as instantaneous input the heat generated by the fuel cell system, the vehicle longitudinal speed, and the current values of temperatures. Each component is then modelled according to energy and mass balances to enable evaluating the corresponding outlet temperatures and electric power consumptions.

Concerning the air compressor, the air mass flow rate and the air pressure are needed to evaluate its contribution in the parasitic power use. The air pressure at the compressor outlet (i.e. the stack inlet) is obtained by interpolating in a one-dimensional experimental lookup table which is provided as a function of the stack current. On the other hand, the air flow rate ($\dot{m}_{air}$) in kilograms per second can be evaluated according to the instantaneous values for stack gross power

and cell voltage using the following equation [33]:

$$\dot{m}_{air} = \frac{3.57e-7 \cdot SR_{air} \cdot P_{stack-gross}}{V_{cell}} \quad (6)$$

where SR_{air} is the air stoichiometric ratio and it is derived from (7) in moles per seconds:

$$\dot{m}_{air*} = \frac{SR_{air} \cdot P_{stack-gross}}{0.21 \cdot 4F \cdot V_{cell}} \quad (7)$$

where 0.21 is the molar proportion of air that is oxygen.

Empirical lookup tables are consequently used to evaluate the adiabatic efficiency ($\eta_{adiabatic}$) and the temperature rise of the compressor as a function of the air flow rate ($\dot{m}_{air}$) and the related ratio between inlet and ambient air pressures (p_{ratio}). Then, the air compressor electric power consumption ($P_{compressor}$) is evaluated using (8):

$$P_{compressor}(\dot{m}_{air}, T_{amb}, p_{ratio})$$
$$= \frac{\dot{m}_{air} \cdot c_{p,air}(T_{amb}) \cdot T_{amb} \cdot p_{ratio}^{\frac{k-1}{k}} - 1}{\eta_{elec} \cdot \eta_{adiabatic}(\dot{m}_{air}, p_{ratio})} \quad (8)$$

where $c_{p,air}$ and k stand for the air specific heat as a function of the ambient temperature T_{amb}, and the specific heat ratio for the air, respectively. η_{elec} is the compressor motor drive electrical efficiency which is assumed having a constant value here.

When it comes to the radiator, two one-dimensional lookup tables are considered that map the heat transfer coefficient between coolant and external air (h_{rad}) as a function of the vehicle speed ($speed_{veh}$) for the radiator fan being activated or de-activated, respectively [34]. The radiator fan state is considered in the binary variable $state_{fan}$. Then, the temperature of the coolant at the radiator outlet ($T_{coolant,out}$) can be calculated as follows:

$$T_{coolant,out}$$
$$= T_{coolant,in} - 0.5$$
$$\cdot \frac{A_{rad} \cdot h_{rad}(speed_{veh}, state_{fan}) \cdot (T_{coolant,in} - T_{amb})}{\dot{m}_{coolant} \cdot c_{p,coolant}} \quad (9)$$

where $T_{coolant,in}$ is the coolant temperature at the radiator inlet and equals the value of coolant temperature at the humidifier outlet in the previous time instant. $\dot{m}_{coolant}$ is the coolant mass flow rate through the coolant pump, while $c_{p,coolant}$ is the specific heat of the coolant. A_{rad} stands for the radiator frontal area, while the 0.5 constant in (9) accounts for the numerical model being initially calibrated for a 0.5 m² radiator. When activated, the radiator fan is assumed here constantly consuming a 300 watts electric power ($P_{radiator-fan}$).

Coolant is circulated through the fuel cell system thanks to the coolant pump, which moves energy through the stack, humidifier, and radiator. The heat exchanged by the humidifier can be determined as follows:

$$Q_{coolant,hum} = \dot{m}_{H_2O} \cdot c_{p,H_2O}$$
$$\cdot (T_{coolant-hum,in} - T_{coolant-hum,out}) \quad (10)$$

where $T_{coolant-hum,in}$ and $T_{coolant-hum,out}$ are the temperatures of coolant into and out the humidifier, respectively. $\dot{m}_{H_2O}$ is the mass flow rate of the coolant water while c_{p,H_2O} is the specific heat for water.

The instantaneous heat removed by the coolant ($Q_{coolant}$) can be calculated using (11):

$$Q_{coolant} = \dot{m}_{coolant} \cdot c_{p,coolant} \cdot (T_{stack} - T_{coolant,out}) \quad (11)$$

From an electrical point of view, the parasitic power consumed by the coolant pump ($P_{coolant-pump}$) can be obtained by interpolating in a one-dimensional lookup table as a function of $\dot{m}_{coolant}$.

The stack temperature in the next time instant ($T_{stack,next}$) can be determined according to the thermal balance reported in (12):

$$T_{stack,next} = T_{stack} + (Q_{stack} - Q_{coolant} - Q_{ambient} - Q_{air}$$
$$- Q_{water-vapor} + Q_{condenser}) \cdot \frac{\Delta t}{L_{lumped}}$$

with

$$Q_{ambient} = h_{stack} \cdot (T_{stack} - T_{amb})$$
$$Q_{air} = \dot{m}_{air} \cdot c_{p,air} \cdot (T_{air,in} - T_{stack})$$
$$Q_{water-vapor} = \dot{m}_{wv-in} \cdot c_{p,wv}(T_{wv,in})$$
$$- \dot{m}_{wv-out} \cdot c_{p,wv}(T_{stack})$$
$$Q_{condenser} = \dot{m}_{H20,condensed} \cdot h_{fg} \quad (12)$$

where Δt and L_{lumped} are the simulation time step in seconds and the lumped stack thermal capacitance in joules per kelvin, respectively. $Q_{ambient}$ is the overall heat transferred from the stack to the ambient by means of natural convection. In this term, h_{stack} is the overall heat transfer coefficient associated with natural convection. Q_{air} is the heat contribution removed by the exhaust air which enters the fuel cell stack at temperature $T_{air,in}$. $Q_{water-vapor}$ accounts for the enthalpy variation of water vapor between inlet and outlet of the stack. In this term, $\dot{m}_{wv-in}$ and $\dot{m}_{wv-out}$ are the mass flow rates of water and vapor entering and exiting the stack, respectively. $c_{p,wv}$ is the corresponding specific heat for water and vapor which is evaluated for temperatures $T_{wv,in}$ and T_{stack}, respectively. $Q_{condenser}$ is the heat exchanged between stack and condenser, which can be evaluated considering the mass flow rate of the condensed water ($\dot{m}_{H20,condensed}$) and the heat of vaporization of water (h_{fg}).

D. NET SYSTEM POWER

The last step of the implemented fuel cell system modelling approach involves determining the net electrical power provided by the system. This is achieved by performing an electrical power balance subtracting the overall auxiliary losses from the system gross power as reported in (13):

$$P_{system-net} = P_{stack-gross} - P_{compressor} - P_{coolant-pump}$$
$$- P_{radiator-fan} - P_{condenser-fan} \quad (13)$$

where $P_{condenser-fan}$ is the power consumption of the condenser fan, which is assumed here being 300 watts when the fuel cell system is in operation.

Finally, the value of $P_{system-net}$ is compared with the net power request evaluated in sub-section II-A. In case of a mismatch, a solver is implemented to iteratively adjust the value of stack current density until comparable values are obtained between the power requested and the power provided. The interested reader can consult [31] to obtain more information regarding the implemented approach for modelling the fuel cell system.

III. OPTIMAL THERMAL MANAGEMENT OF FUEL CELL SYSTEMS IN ELECTRIFIED VEHICLES

This section describes the methodology for assessing the potential of optimal control when applied to the thermal management of fuel cell systems in FCEVs. The high-level workflow of the proposed methodology is shown in Fig. 3. The inputs of the analysis are the vehicle speed and the net fuel cell system power request in the entire driving mission as it has been described in section II-C. Then, two FCEV thermal management approaches are implemented in parallel that take the same inputs. On one hand, DP is considered as global optimal control reference requiring the a priori knowledge of the entire driving mission. On the other hand, a baseline reactive control strategy is implemented. Forward simulations of the fuel cell system model described in section II are performed for both the considered control approaches. Obtained results allow to compare DP and the baseline reactive control approach for different lengths of driving mission and ambient temperatures. FCEV energy balance and operational statistics are assessed along with evaluating the hydrogen saving potential predicted by DP. The rest of this section is organized as follows: the optimal control problem formulation for thermal management of automotive fuel cell systems is illustrated first. Finding the global optimal solution for the introduced control problem in an off-line approach is then discussed by implementing dynamic programming (DP). The final sub-section describes the reactive control approach which is used as reference for benchmarking the potential of optimal thermal management for fuel cell systems in terms of hydrogen saving.

A. OPTIMAL CONTROL PROBLEM
Here, the optimal control problem for thermal management of fuel cell systems in FCEVs aims at minimizing the hydrogen consumption while simultaneously complying with operative and thermal constraints for the fuel cell stack and the components of the auxiliary system. The proposed control problem along with the optimization constraints are described in (14).

$$\arg \min \left\{ J = \int_{t_0}^{t_{end}} \dot{m}_{H2} \left[P_{stack-gross}(t), state_{fan}(t), \right. \right.$$
$$\left. \left. \dot{m}_{coolant}(t), t \right] dt \right\} \quad (14)$$

Subject to :

Fuel cell stack constraints:
$$T_{stack}(t) \leq T_{stack-lim} \quad (15)$$
$$P_{system-net}(t) \geq P_{system-request}(t)$$
Radiator fan constraint:
$$state_{fan}[(t, speed_{veh}(t) = 0)] = 0 \quad (16)$$
Coolant pump constraints:
$$\dot{m}_{coolant}[(t, speed_{veh}(t) = 0)] = 0$$
$$\dot{m}_{coolant-min} \leq \dot{m}_{coolant}(t) \leq \dot{m}_{coolant-MAX} \quad (17)$$

The cost function J to be minimized includes the hydrogen consumption in the overall driving mission from the initial time instant t_0 up to the final time instant t_{end}. Concerning stack constraints in (15), the value of stack temperature over time as evaluated using (12) is prevented to exceed the operational limit $T_{stack-lim}$ which is assumed being 95 °C here. The net power provided by the fuel cell system as evaluated using (13) needs to never be lower than the corresponding power request coming from the FCEV supervisory control logic. Indeed, a lower value of power provided by the fuel cell system would lead to deplete the battery state-of-charge, which would in turn counteract the control decision taken by the FCEV control logic. As a general reminder, the FCEV supervisory control logic is responsible for deciding upon the power split between the fuel cell system and the battery pack at each time instant, while the control logic considered in this work is responsible for controlling the fuel cell system and its auxiliary components in a lower-level approach based on the input provided by the FCEV supervisory control logic. In this work, the high-level FCEV supervisory control logic is a rule-based thermostatic strategy inherited from Advisor™ 2003. The controlled components of the thermal system of the fuel cell (i.e. radiator fan and coolant pump in this case) are prevented from being activated if the vehicle is not in motion in (16) and (17) in order not to potentially undermine passenger acoustic comfort. Finally, the coolant mass flow rate value is constrained within the physical operational limits of the coolant pump in (17). In this framework, subscripts 'min' and 'MAX' respectively denote lower and upper operational boundaries.

B. OPTIMAL THERMAL MANAGEMENT OF FUEL CELL SYSTEMS USING DYNAMIC PROGRAMMING
The core idea of this work relates to assess the global optimal solution for the introduced thermal control problem of fuel cell systems. This section describes the methodology implemented for evaluating the global optimal control solution which relies on dynamic programming (DP). DP is one of the most common approaches to evaluate the global optimal solution for a given dynamic control problem [35], [36]. DP requires a priori knowledge of the entire time horizon of the considered control problem, i.e., the entire driving mission in terms of vehicle speed and fuel cell system power request over time in this case. This allows DP to find the
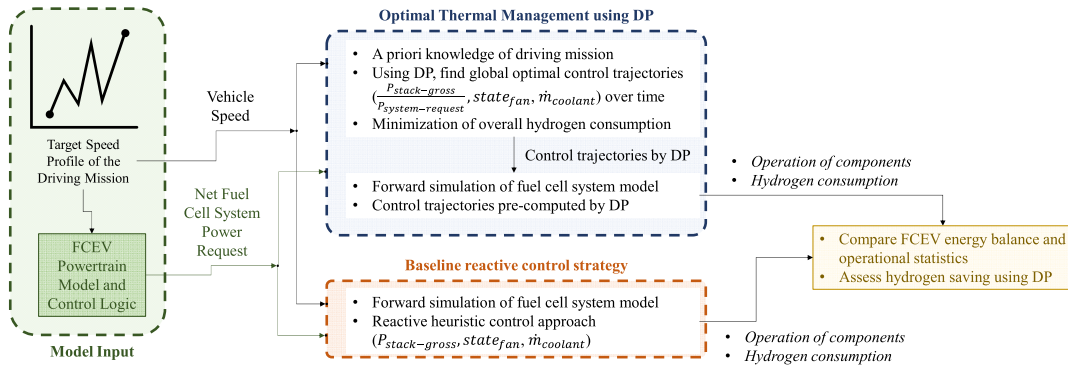
global optimal solution for the proposed control problem in an off-line approach [37], [38]. Discretized arrays for control variables and state variables need definition in DP [39]. Control variables are directly managed by the control system under consideration. On their behalf, state variables characterize by their values being tracked and updated throughout the driving mission under analysis [40], [41]. The full control variable set U and the state variable set X for the fuel cell system thermal control problem under investigation are illustrated in (18):

$$U = \left\{ \begin{array}{c} \frac{P_{stack-gross}}{P_{system-request}} \\ state_{fan} \\ \dot{m}_{coolant} \end{array} \right\} ; X = \left\{ \begin{array}{c} T_{stack} \\ T_{coolant} \end{array} \right\} \quad (18)$$

The implemented DP version involves controlling the ratio between fuel cell system gross power and the corresponding net power request coming from the FCEV supervisory control logic, along with the radiator fan state and the coolant mass flow rate provided by the pump. On the other hand, X includes the temperature values for both the stack and the coolant. In this way, stack and coolant temperatures can appropriately be updated at each time instant throughout the driving mission according to (12) and (9), respectively. The open source 'DynaProg' DP function implemented in Matlab® is used in this work for solving the illustrated optimal control problem for thermal management of fuel cell systems [42].

C. BASELINE REACTIVE CONTROL STRATEGY

After implementing DP and finding the global optimal solution for the fuel cell system thermal control problem, the following step involves quantifying the hydrogen saving capabilities compared with a reference approach. Here, the reference approach relates to the real-time capable fuel cell thermal management strategy available in Advisor™ 2003 [31]. Similarly with DP, the baseline reactive thermal control strategy is required to set at each time instant the values for the radiator fan state, the coolant mass flow rate provided by the pump, and the gross power of the fuel cell stack.

The baseline reactive control strategy activates the radiator fan as soon as the value of stack inlet temperature exceeds the operating temperature set point, which corresponds to 80 °C. Then, the radiator fan is kept operating as long as the value of stack inlet temperature is greater than 80°.

As far as the thermal pump is concerned, one of its operating requirements involves limiting the temperature rise across the fuel cell for practical reasons. The baseline reactive thermal control strategy assumes that all the internal energy generated is transferred to the coolant. Then, the coolant mass flow rate in kilograms per second can be determined as follows:

$$\dot{m}_{coolant} = \frac{Q_{stack}}{c_{p,coolant} \cdot \Delta T_{allowed}} \quad (19)$$

where $\Delta T_{allowed}$ is the maximum amount of temperature rise that the fuel cell can tolerate, which is calibrated as 8 °C for the vehicle considered in Advisor™ 2003.

The final control variable is the fuel cell stack gross power, which is iteratively adjusted in the baseline reactive control strategy until the net power provided by the fuel cell system as evaluated in (13) fulfills the corresponding vehicle power request. Further details were reported in sub-section II-D in this paper.

IV. RESULTS

In this section, numerical results are presented for a case study regarding the optimal thermal management of fuel cell systems in electrified vehicles.

Table 2 shows the applied discretization grids for both control and state variables, where the number of elements for each variable has been decided aiming at the right trade-off between discretization accuracy and overall computational cost for running DP.

From the thermal management point of view, DP controls the state of the radiator fan and the coolant mass flow rate. Several DP simulations are performed here by sweeping two parameters: 1) the number of steady repetitions of WLTC, which is set from 1 to 10 to consider up to 234km driven in a single driving mission; 2) the ambient temperature, which is

TABLE 2. Discretized control and state variables in DP.

Type	Parameter	Value	Units of measure
Control variables	$\dfrac{P_{stack-gross}}{P_{stack-request}}$	(1 : 0.02 : 1.4)	[-]
State variables	$state_{fan}$	[0 1]	[-]
	$\dot{m}_{coolant}$	[0 0.05 0.1 0.15 0.2 0.3 0.4 0.5 1 1.5]	kg/s
	T_{stack}	$(T_{amb} : 0.5 : 100)$	°C
	$T_{coolant}$	$(T_{amb} : 0.5 : 100)$	°C

set from $-20\,°C$ to $40\,°C$ considering a $5\,°C$ temperature step. The driving mission is discretized over time with 1 second steps, while the initial stack temperature is set to be equal to the ambient temperature. Once the control trajectories over time are generated by DP for the entire driving mission, these are fed to a forward model of the fuel cell system to evaluate the time series of stack and coolant temperatures along with overall energy consumption values in the driving mission. This allows evaluating energy and thermal balances while avoiding the dependence of the DP simulation results on the discretization of state variables. Table 3 reports the hydrogen consumption for both the global optimal solution obtained by DP and for the baseline reactive control strategy as a function of the ambient temperature and the trip length, along with the percentage difference between the two values. Values of ambient temperature equal to $-20\,°C$, $10\,°C$ and $40\,°C$ are considered being respectively representative of cold weather ('LoTe'), mild weather ('MeTe'), and hot weather ('HiTe'). On the other hand, short trip ('ShTr'), medium trip ('MeTr'), and long trip ('LoTr') relate to 1 WLTC repetition (i.e. around 23 km), 3 WLTC repetitions (i.e. around 47 km), and 10 WLTC repetition (i.e. around 233 km), respectively. Compared with the baseline reactive control strategy, the optimal off-line benchmark exhibits up to a significant 10.2% hydrogen saving capability corresponding to a short trip performed in cold ambient temperature. On the other hand, the hydrogen saving capability compared with the baseline reactive control approach gradually decreases both when the trip length and the ambient temperature increase, respectively. Low temperatures are the only exception in this case, since a medium trip would entail less energy saving capability compared with a long trip. Fig. 4 shows the full spectrum of percentage hydrogen saving capability of the global optimal solution compared with the baseline reactive control strategy as a function of the ambient temperature and the trip length. In particular, the number of steady repetitions of WLTC has been varied from 1 to 10 and the ambient temperature has been varied from $-20\,°C$ to $40\,°C$ with a $5\,°C$ step for both DP and baseline reactive control logic. Then, Fig. 4 has been created by interpolating between the discrete simulation results obtained.

As further evaluation metrics, Fig. 5 and Fig. 6 illustrate the percentages of the driving mission time in which the radiator and the coolant pump are in operation according to both Advisor and DP control logics, respectively. Looking at Fig. 5 (a), DP can reduce the radiator operational time by one order of magnitude at cold ambient temperature for all the examined trip lengths, thus drastically reducing the associated parasitic losses. A similar trend can be observed in Fig. 5 (b) for $10\,°C$ ambient temperature, while the activation time of the radiator by DP at $40\,°C$ ambient temperature is 27% to 43% of the value corresponding to the baseline reactive control strategy, depending on the trip length. As regards Fig. 6, the baseline reactive control approach implemented in Advisor sets the coolant pump to be always activated when the vehicle is moving, thus involving the associated parasitic loss to be constantly positive. On the other hand, the proposed DP approach tends to turn off the coolant pump, when possible, which allows to reduce the parasitic loss associated. Also in this case, the operational time of the coolant pump set by DP is around one order of magnitude less than the value corresponding to the baseline reactive control approach for each of the analyzed trip lengths at $-20\,°C$ and $10\,°C$. The operational time reduction for the coolant pump achieved by DP gets reduced for $40\,°C$ ambient temperature and is even higher than the corresponding value by Advisor for WLTCx10. A more comprehensive explanation for this behavior will be provided in Section IV-C.

An in-depth analysis of simulation results for the driving missions being performed at low ambient temperature, mild ambient temperature and hot ambient temperature will be performed in the follow up of this section, respectively.

A. RESULTS ANALYSIS FOR COLD AMBIENT TEMPERATURE

Fig. 7 illustrates statistics in terms of energy loss and fuel cell system efficiency for the FCEV simulated at $-20\,°C$ ambient temperature being controlled by both DP and the baseline reactive control strategy inherited from Advisor. Moreover, simulation time series of vehicle control and state variables are shown in Fig. 10 to Fig. 12 in Appendix A.1 along with the entire set of energy statistics for the simulations reported in Table 4.

Looking at Fig.7 in Appendix A.1, the optimal thermal control benchmark found by DP involves drastically reducing the operational time and the auxiliary power consumption of the coolant pump. For example, around 550kJ can be saved in the optimal thermal control solution provided by DP in WLTCx1 as shown in Fig. 7(a). Moreover, a further beneficial side effect can be achieved in this way at low ambient temperatures. Indeed, reducing the operation of the coolant pump leads the fuel cell stack temperature to noticeably increase by around $20\,°C$ on average over time compared with the baseline reactive control strategy provided by Advisor. Rising the average stack operational temperature entails increasing the efficiency both stack and fuel cell system levels by few percentage points, as it has been illustrated in Fig. 7(a).
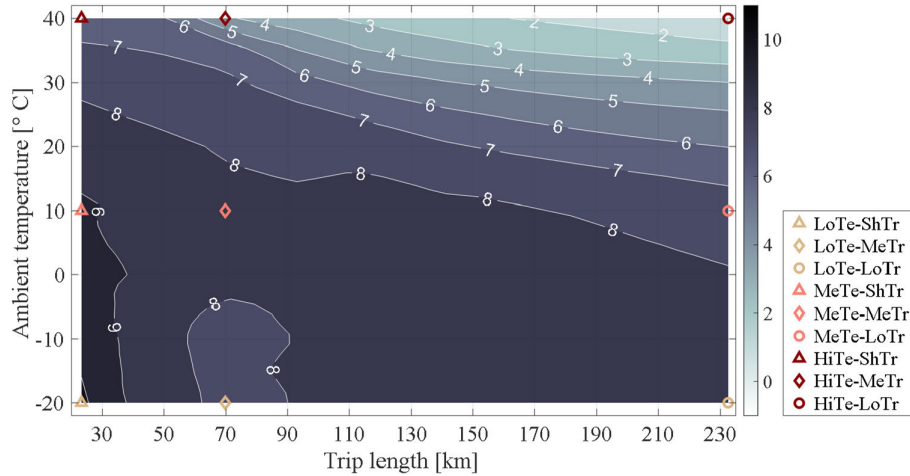
FIGURE 4. Percentage hydrogen saving for DP compared with the baseline reactive thermal control strategy as a function of trip length and ambient temperature.

TABLE 3. Hydrogen consumption corresponding to the global optimal solution ('DP') and the baseline reactive control strategy ('Advisor') as a function of the ambient temperature and the trip length (considering steady repetitions of WLTC).

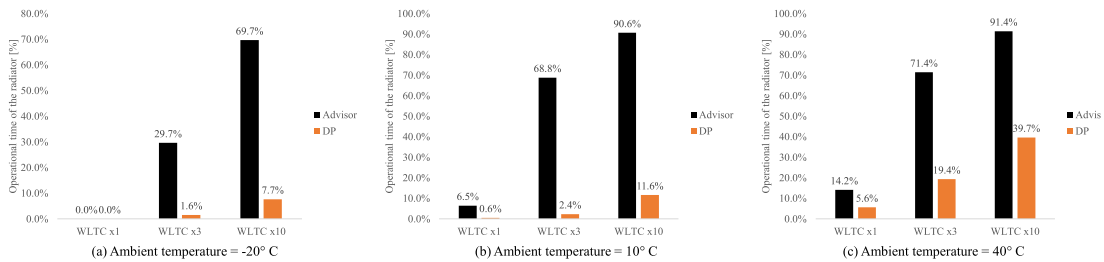| Ambient temperature	Short trip 'ShTr'(WLTCx1)		Medium trip 'MeTr' (WLTCx3)		Long trip 'LoTr' (WLTCx10)	
	Advisor [kg/100 km]	DP [kg/100 km]	Advisor [kg/100 km]	DP [kg/100 km]	Advisor [kg/100 km]	DP [kg/100 km]
-20 °C ('LoTe')	1.07	0.96 (-10.2%)	1.01	0.93 (-7.9%)	0.99	0.90 (-8.4%)
10 °C ('MeTe')	1.05	0.94 (-9.1%)	1.00	0.92 (-8.3%)	0.99	0.91 (-7.5%)
40 °C ('HiTe')	1.00	0.93 (-6.5%)	0.98	0.94 (-4.1%)	0.97	0.96 (-1.4%)

FIGURE 5. Operational time of the FCEV radiator for both DP and the baseline reactive thermal control strategy as a function of trip length and ambient temperature.
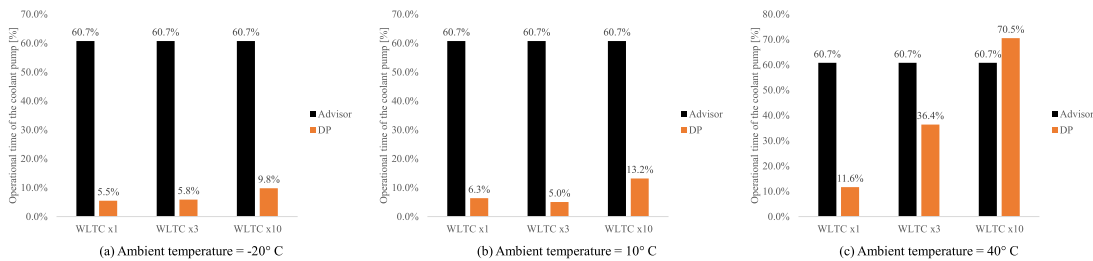

FIGURE 6. Operational time of the FCEV coolant pump for both DP and the baseline reactive thermal control strategy as a function of trip length and ambient temperature.

A further action taken by DP at low ambient temperature is shown in the optimal control solution in Fig. 10. DP chooses to operate the coolant pump at around 1.5kg/s coolant rate in the first 200 seconds of WLTC. This has a minor impact on the temperature values for the stack and the coolant since they are both around −20 °C at the beginning of the journey.
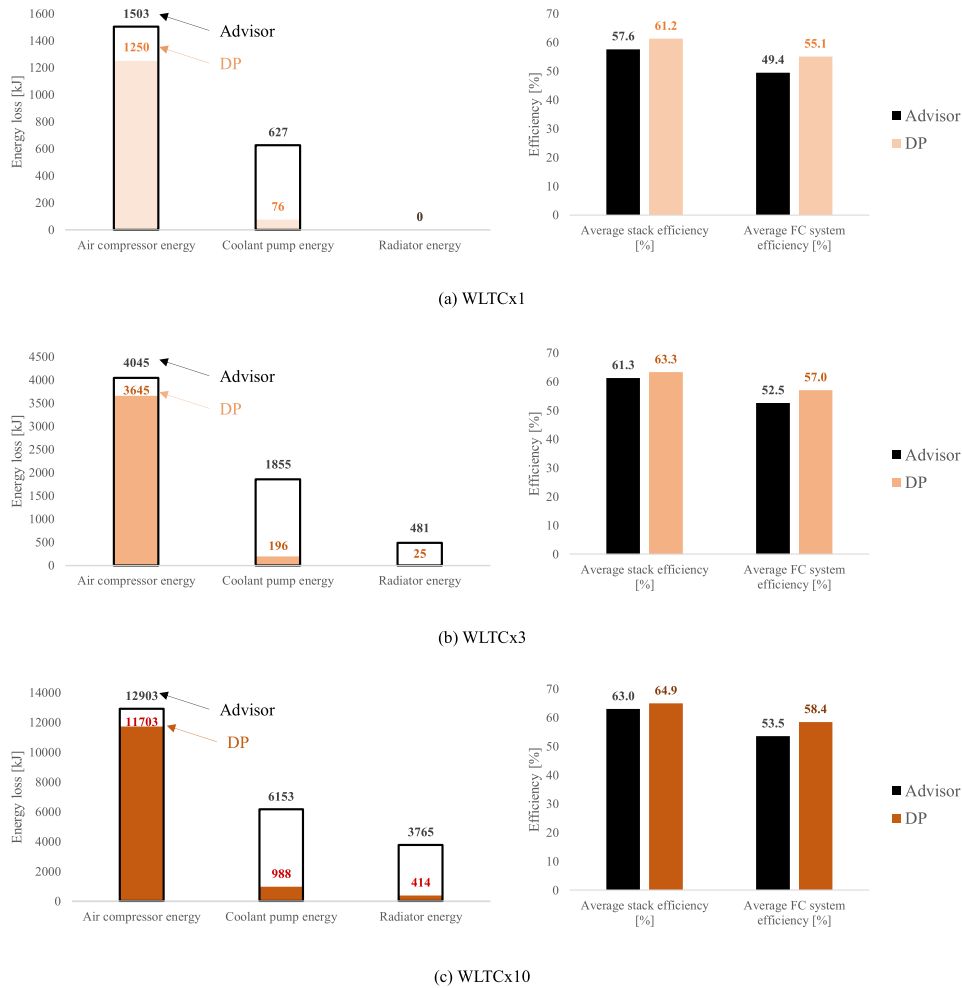
(a) WLTCx1

(b) WLTCx3

(c) WLTCx10

FIGURE 7. Statistics in terms of energy loss and fuel cell system efficiency for the FCEV simulated at −20° C ambient temperature being controlled by both DP and the baseline reactive control strategy from Advisor in WLTCx1, WLTCx3 and WLTCx10 driving missions.

TABLE 4. Energy statistics for the fuel cell system simulated being controlled by DP and by the baseline reactive control strategy from Advisor over different numbers of WLTC repetitions at −20 °C ambient temperature.

		WLTCx1		WLTCx3		WLTCx10	
		Advisor	DP	Advisor	DP	Advisor	DP
Energy loss [kJ]	Air compressor energy	1503	1250	4045	3645	12903	11703
	Coolant pump energy	627	76	1855	196	6153	988
	Radiator energy	0	0	481	25	3765	414
	Condenser fan energy	328	328	985	985	3282	3282
	Chemical loss	12646	10381	32613	28482	102097	88502
Statistics	Net energy generation [kJ]	14745	14745	44234	44234	147446	147446
	Gross energy generation [kJ]	17171	16399	51569	49079	173519	163827
	Average stack efficiency [%]	57.6	61.2	61.3	63.3	63.0	64.9
	Average FC system efficiency [%]	49.4	55.1	52.5	57.0	53.5	58.4
	H2 consumption [kg]	0.25	0.22	0.70	0.65	2.30	2.10
	Driving mission length [km]	23.4	23.4	70.2	70.2	234.0	234.0
	Predicted H2 economy [kg/100 km]	1.06	0.95	1.00	0.92	0.98	0.90

However, the auxiliary power consumption of the coolant pump increases the gross power produced by the fuel cell system Q_{stack}, which in turn entails an overall higher stack temperature rise following (9). Consequently, the stack can

(a) WLTCx1
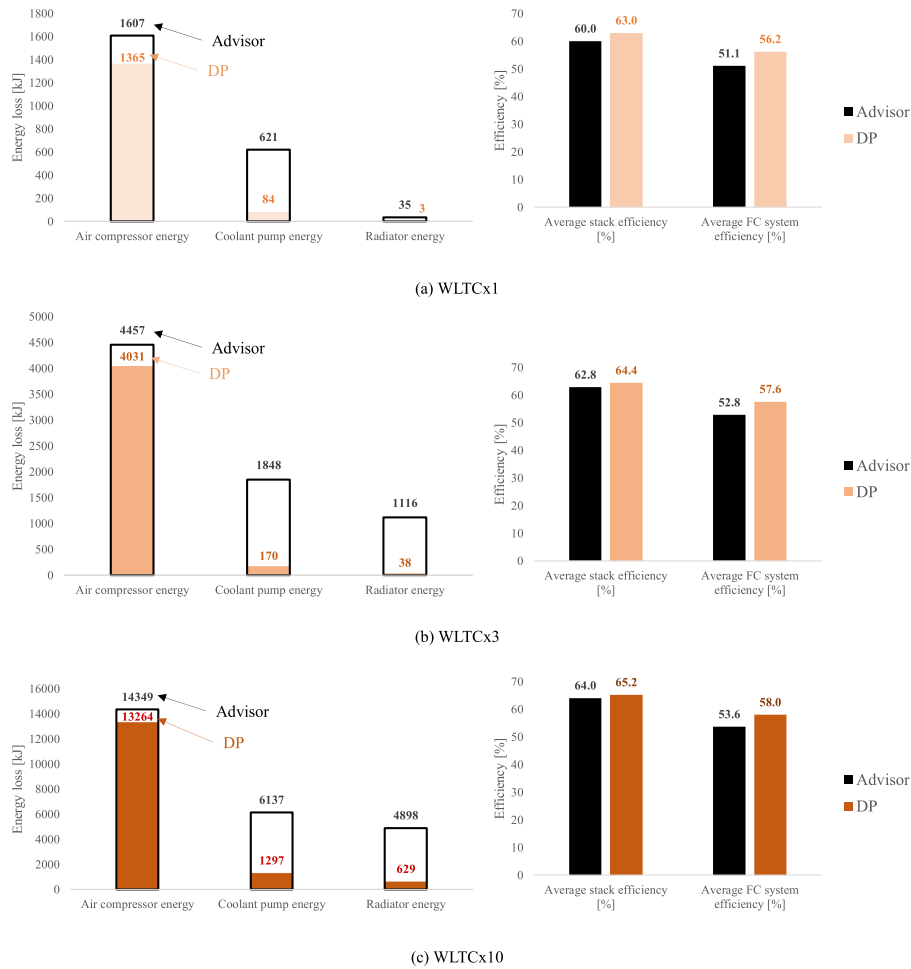

(b) WLTCx3

(c) WLTCx10

FIGURE 8. Statistics in terms of energy loss and fuel cell system efficiency for the FCEV simulated at 10° C ambient temperature being controlled by both DP and the baseline reactive control strategy from Advisor in WLTCx1, WLTCx3 and WLTCx10 driving missions.

reach efficient operating regions which relate to higher operating temperatures sooner in the driving mission.

As it can be seen in Fig. 7, the air compressor is the most energy demanding auxiliary component of the fuel cell system. Its air mass flow rate is not considered here as a variable controlled by DP, but rather its value over time is set according to the baseline reactive control approach. However, reducing the gross power required by the fuel cell system is demonstrated to bring significant benefits concerning the power consumption of the air compressor as it was shown in (5) and in (6) in Section II-C. Such virtuous loop can be listed among the key benefits brought by the proposed optimal thermal control approach in terms of hydrogen saving.

When considering medium distance (e.g. WLTCx3) and long distance (e.g. WLTCx10) driving missions at low ambient temperatures, the global optimal thermal control solution provided by DP is suggested to operate in a similar way compared to a short driving mission (e.g. WLTCx1). Significant reductions in the use of the coolant pump can be noticed in Fig. 7(b) and in Fig. 7(c) for DP compared with the baseline reactive controller from Advisor. Moreover, early activation

of the coolant pump in the driving mission can be seen in Fig. 11 and in Fig. 12. Nevertheless, higher hydrogen saving is suggested in Fig. 4 to be achieved by DP compared with the baseline reactive controller in a long-distance trip than in a medium-distance trip. A possible explanation can be provided looking at Fig. 12 in Appendix A.1 and noticing that the fuel cell stack operates at higher temperatures (e.g. around 90 °C) for a higher time share in the 230km long driving mission, which improves the overall hydrogen saving capability for the fuel cell system. Higher travel distances (e.g. few hundreds kilometers) at low ambient temperatures are thus suggested to offer enhanced potential for hydrogen saving in FCEVs compared with medium travel distances (e.g. lower than 100 kilometers).

B. RESULTS ANALYSIS FOR MILD AMBIENT TEMPERATURE

Fig. 8 shows statistics in terms of energy loss and fuel cell system efficiency for the FCEV simulated at 10 °C ambient temperature being controlled by both DP and the baseline reactive control strategy inherited from Advisor. Moreover,
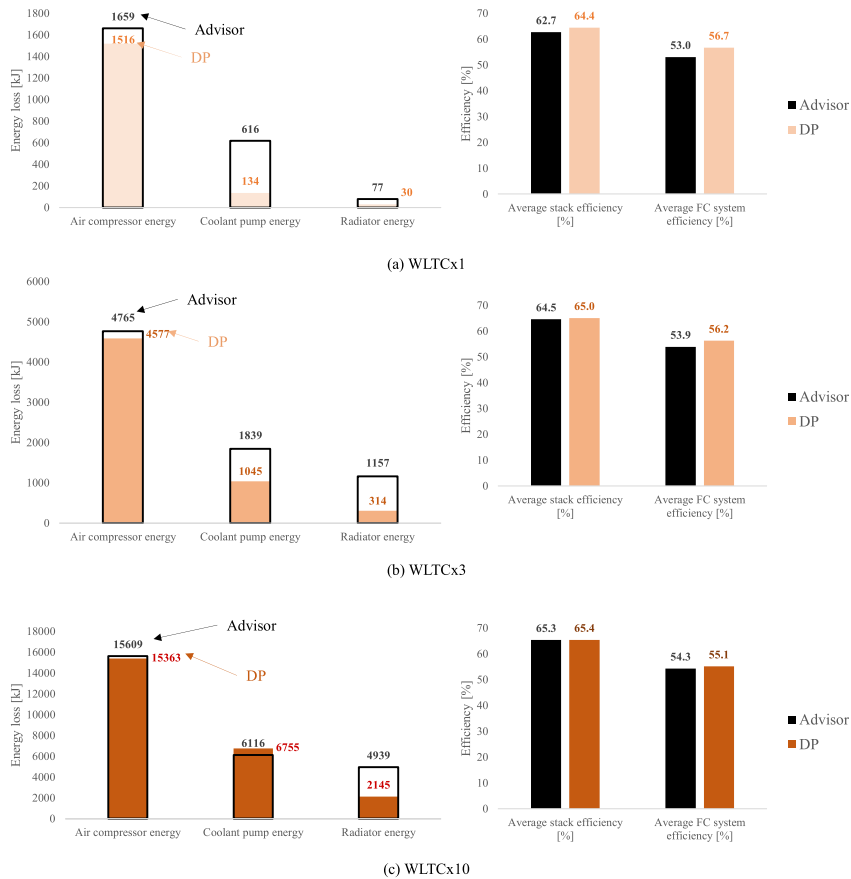
(a) WLTCx1

(b) WLTCx3

(c) WLTCx10

FIGURE 9. Statistics in terms of energy loss and fuel cell system efficiency for the FCEV simulated at 40° C ambient temperature being controlled by both DP and the baseline reactive control strategy from Advisor in WLTCx1, WLTCx3 and WLTCx10 driving missions.
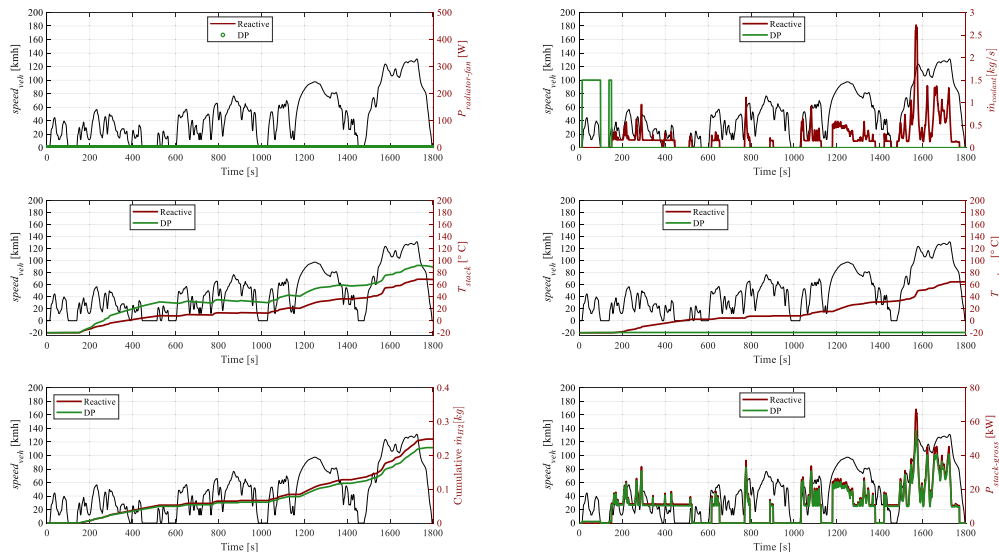

FIGURE 10. Time series of control and state variables for the FCEV simulated at −20 °C ambient temperature being controlled by both DP and the baseline reactive control strategy from Advisor in WLTCx1.

simulation time series of vehicle control and state variables are illustrated in Fig. 13 to Fig. 15 in Appendix A.2 along with the entire set of energy statistics for the simulations reported in Table 5.

Overall, simulations performed considering mild ambient temperatures suggest as well that the highest share of hydrogen saving capability for the optimal thermal control benchmark of the FCEV relates to the coolant pump. Indeed, the
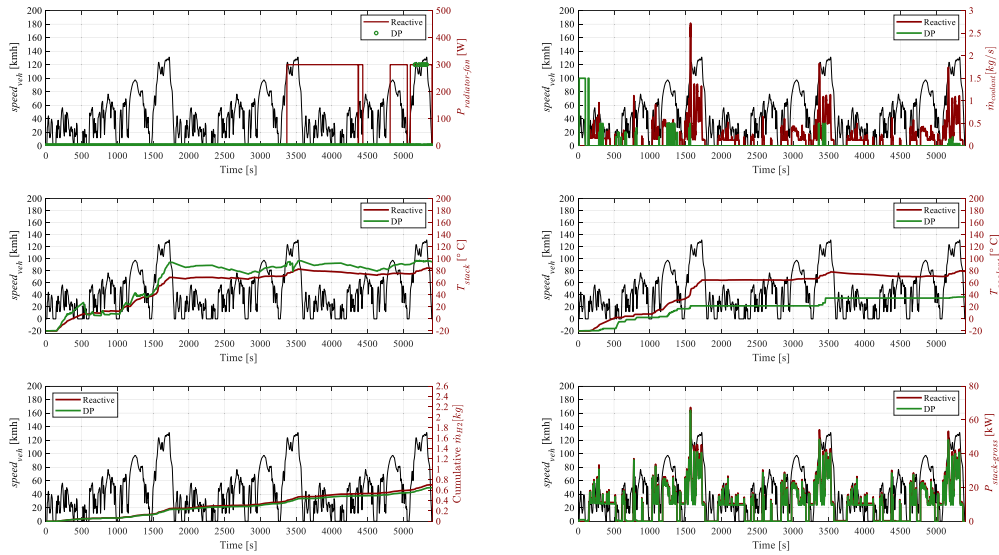
FIGURE 11. Time series of control and state variables for the FCEV simulated at −20 °C ambient temperature being controlled by both DP and the baseline reactive control strategy from Advisor in WLTCx3.

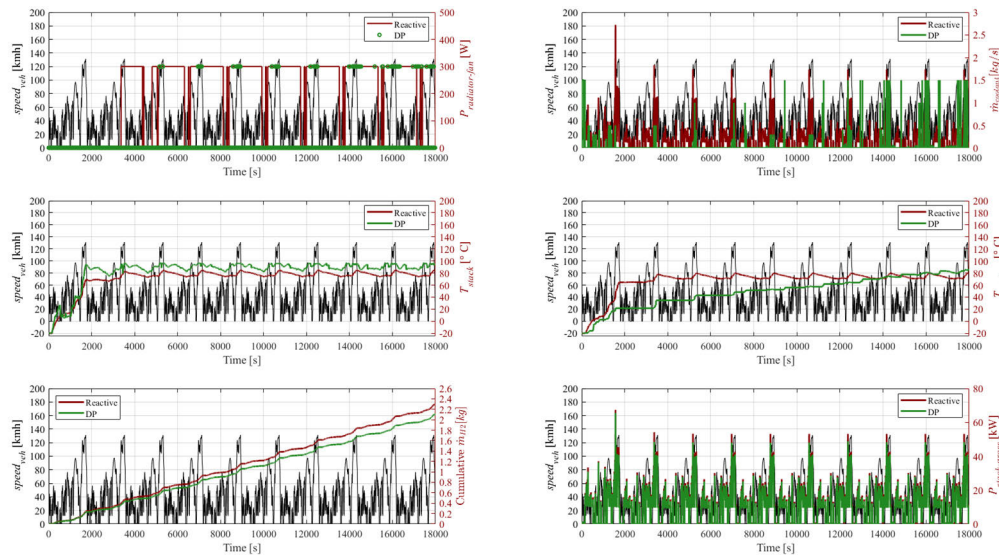**FIGURE 12.** Time series of control and state variables for the FCEV simulated at −20 °C ambient temperature being controlled by both DP and the baseline reactive control strategy from Advisor in WLTCx10.

auxiliary power consumption of the coolant pump throughout the driving mission being controlled by DP is one order of magnitude lower compared with the corresponding metric for the baseline reactive controller simulation both in short, medium, and long trips in Fig. 8. The same consideration holds for the auxiliary energy consumed by the radiator fan although its overall energy consumption is less impactful compared with the coolant pump term in Fig. 8.

The DP simulation results for the short trip (i.e. WLTCx1) at 10°C ambient temperature shown in Fig. 13 suggest a similar behavior for the optimal thermal control benchmark compared with the cold temperature case which was assessed in the previous paragraph. Indeed, enhancing the overall fuel

cell system efficiency is achieved by reducing the ON time of both the coolant pump and the radiator fan, along with reducing the coolant mass flow rate over time in general. Moreover, higher stack temperatures are attained in Fig. 13 by DP compared with the baseline reactive controller, which results in higher stack efficiency as illustrated in Fig. 8 (a).

When the length of the trip increases, reduced utilization of the radiator fan and the coolant pump are predicted as hydrogen saving enablers by DP in Fig. 14 and in Fig. 15 as well. In particular, the optimal control behavior predicted by DP is observed remarkably reducing the overall radiator fan ON time in medium and long trips at mild ambient temperatures compared with the baseline reactive control
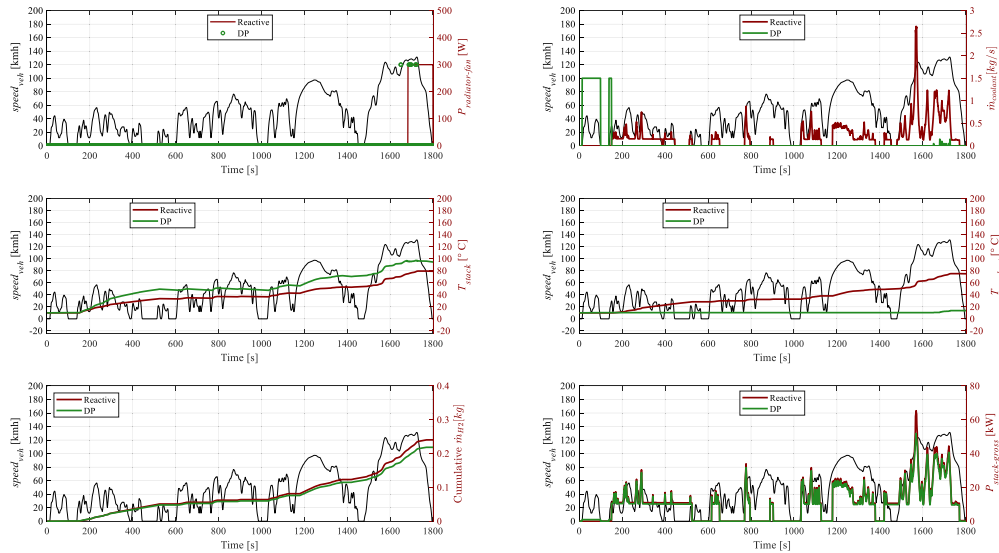
FIGURE 13. Time series of control and state variables for the FCEV simulated at 10 °C ambient temperature being controlled by both DP and the baseline reactive control strategy from Advisor in WLTCx1.

FIGURE 14. Time series of control and state variables for the FCEV simulated at 10 °C ambient temperature being controlled by both DP and the baseline reactive control strategy from Advisor in WLTCx3.
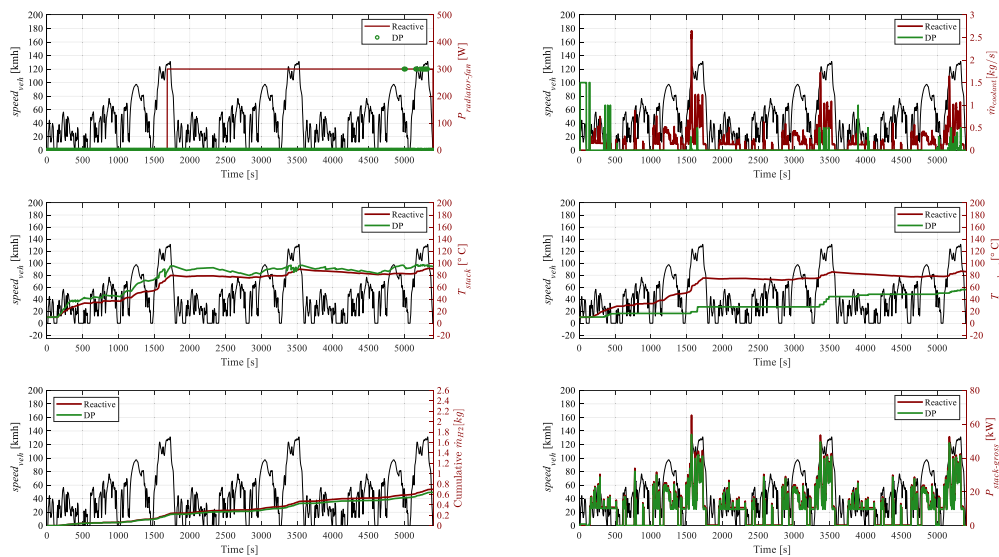
strategy. Moreover, DP activates the radiator fan in Fig. 14 and in Fig. 15 only at high values of vehicle speed as in highway driving, which considerably improves the efficiency of the heat removal process within the radiator. For example, the overall radiator energy consumption predicted by DP in WLTCx3 reported in Fig 5(b) is 3.4% only compared with the corresponding metric related to the baseline reactive control approach provided by Advisor.

C. RESULTS ANALYSIS FOR HOT AMBIENT TEMPERATURE
Fig. 9 illustrates statistics in terms of energy loss and fuel cell system efficiency for the FCEV simulated at 40 °C ambient temperature being controlled by both DP and the baseline

reactive control strategy inherited from Advisor. Moreover, simulation time series of vehicle control and state variables are illustrated in Fig. 16 to Fig. 18 in Appendix A.3 along with the entire set of energy statistics for the simulations reported in Table 6. As previously illustrated in Fig. 4, hot ambient temperatures offer a relatively limited potential for hydrogen saving via optimal control given the restricted freedom in the operation of the thermal controller. Indeed, 6.5% hydrogen consumption reduction has been suggested at maximum compared with the baseline reactive thermal control approach.

Looking at Fig. 16, DP chooses to activate the radiator fan at high values of vehicle speed as it was performed at mild ambient temperatures. However, the baseline reactive controller activates the radiator fan during highway driving too as
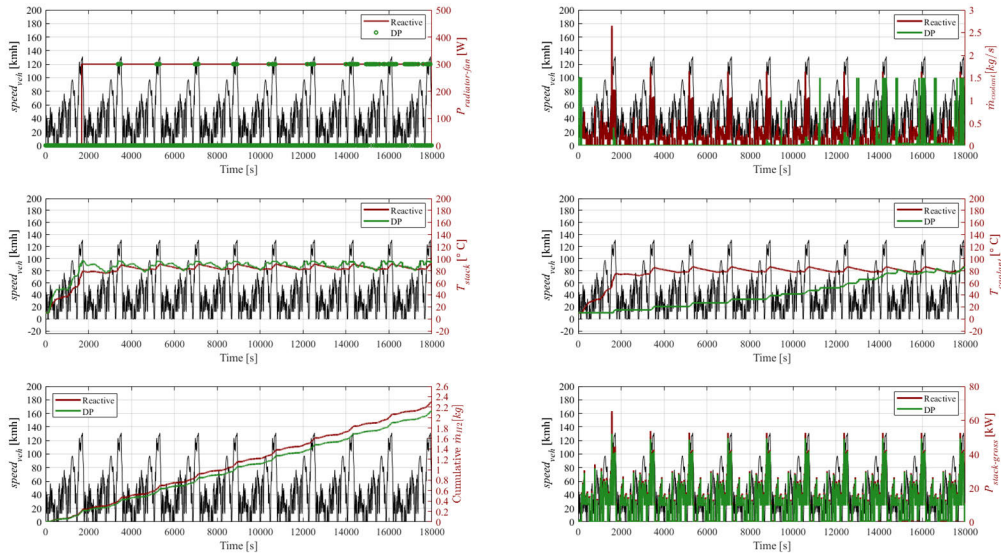
FIGURE 15. Time series of control and state variables for the FCEV simulated at 10 °C ambient temperature being controlled by both DP and the baseline reactive control strategy from Advisor in WLTCx10.

TABLE 5. Energy statistics for the fuel cell system simulated being controlled by DP and by the baseline reactive control strategy from Advisor over different numbers of WLTC repetitions at 10 °C ambient temperature.

		WLTCx1		WLTCx3		WLTCx10	
		Advisor	DP	Advisor	DP	Advisor	DP
Energy loss [kJ]	Air compressor energy	1607	1365	14349	13264	14349	13264
	Coolant pump energy	621	84	6137	1297	6137	1297
	Radiator energy	35	3	4898	629	4898	629
	Condenser fan energy	328	328	3282	3282	3282	3282
	Chemical loss	11548	9709	98869	88452	98869	88452
Statistics	Net energy generation [kJ]	14745	14745	147446	147446	147446	147446
	Gross energy generation [kJ]	17328	16525	176103	165917	176103	165917
	Average stack efficiency [%]	60.0	63.0	64.0	65.2	64.0	65.2
	Average FC system efficiency [%]	51.1	56.2	53.6	58.0	53.6	58.0
	H2 consumption [kg]	0.24	0.22	2.29	2.12	2.29	2.12
	Driving mission length [km]	23.4	23.4	70.2	70.2	234.0	234.0
	Predicted H2 economy [kg/100 km]	1.03	0.93	3.26	3.02	0.98	0.91

the stack temperature exceeds 80 °C at around 1550 seconds in WLTCx1. Therefore, limited radiator auxiliary energy reduction is observed being achievable via optimal control in Fig. 9(a) compared with the remaining simulation cases. As regards the coolant pump, limiting its operation is suggested by DP in short trips at high ambient temperatures as well. Even in this case, DP chooses to activate the coolant pump in the first phases of WLTCx1 to allow the stack attaining efficient operation at high temperatures earlier in Fig. 16.

Medium distance and long-distance trips at 40 °C are the most demanding scenarios for the fuel cell system form a thermal perspective. In Fig. 17, DP chooses to activate both

the coolant pump and the radiator fan at around 2200 seconds to limit the stack temperature increase. Therefore, the stack temperature exhibits similar values between DP and the baseline reactive controller in the second repetition of WLTC. Here, the third WLTC repetition in Fig. 17 is the only case in which DP chooses to maintain the stack temperature lower compared with the baseline reactive controller. This is achieved by DP through keeping the radiator fan activated for long and through an intense use of the coolant pump in the final phases of the driving mission. This motivates the higher energy losses for the coolant pump and the radiator fan in Fig. 9 (b) compared with both Fig. 7(b) and Fig. 8(b). Nevertheless, the potential benefit of the optimal thermal control
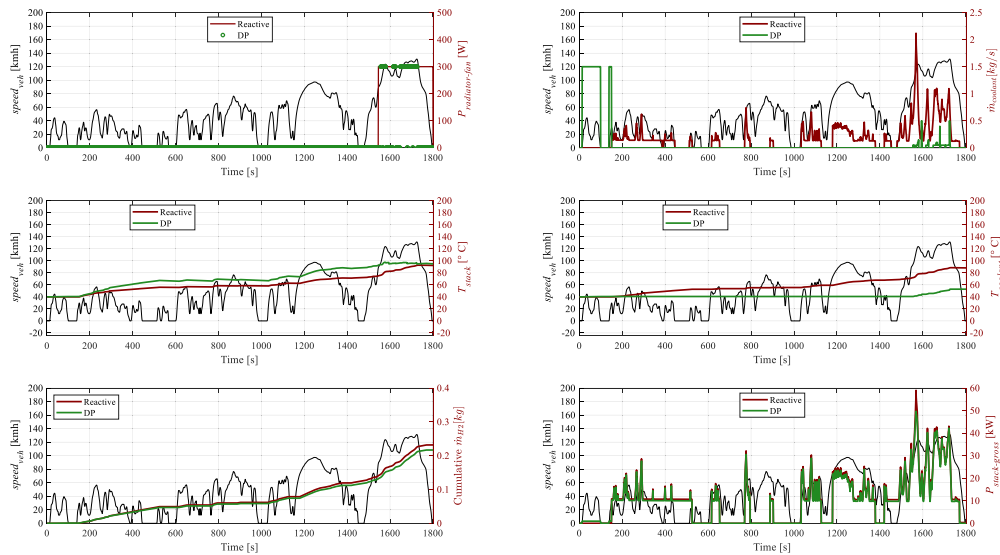
FIGURE 16. Time series of control and state variables for the FCEV simulated at 40 °C ambient temperature being controlled by both DP and the baseline reactive control strategy from Advisor in WLTCx1.

FIGURE 17. Time series of control and state variables for the FCEV simulated at 40 °C ambient temperature being controlled by both DP and the baseline reactive control strategy from Advisor in WLTCx3.
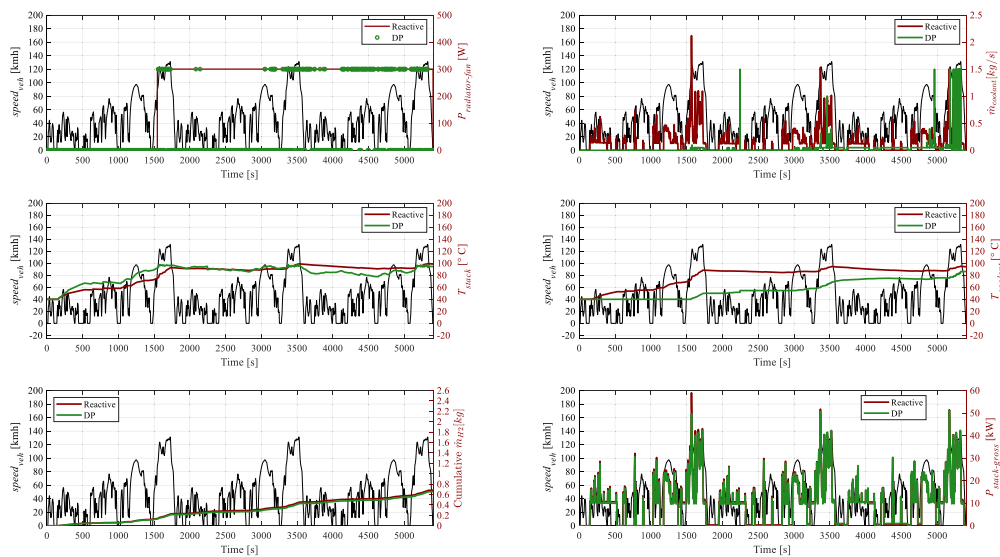
benchmark is preserved since DP predicts 4.1% hydrogen saving.

When it comes to long-distance trips performed at high ambient temperatures, DP chooses on average to keep the stack colder compared with the baseline reactive control strategy in Fig. 18. This is mostly performed through an intense use of the coolant pump, whose electric energy consumption reported in Fig. 9(c) is even higher by around 640kJ (10.5%) compared with the baseline reactive controller. Indeed, the largest share of hydrogen saving potential in long trips at high ambient temperatures is predicted to be achieved by reducing the overall ON time of the radiator fan, particularly in the second WLTC repetition in Fig. 18. Thanks to this strategy, the electric energy consumption of the radiator fan can be cut down by around 2800kJ in the optimal control solution compared with the baseline reactive control strategy.

V. CONCLUSION

This paper has discussed the optimal thermal management of automotive fuel cell system. Particularly, the study focused on the optimization of the fuel cell system performance at various operating conditions for both short- and long-term driving missions. The electrochemical and thermal models of a fuel cell system for automotive applications have been considered. Then, DP has been implemented as global optimal thermal management approach. The control variables involved the gross stack power, the radiator fan state, along with the coolant flow rate circulating in the coolant pump. Numerical
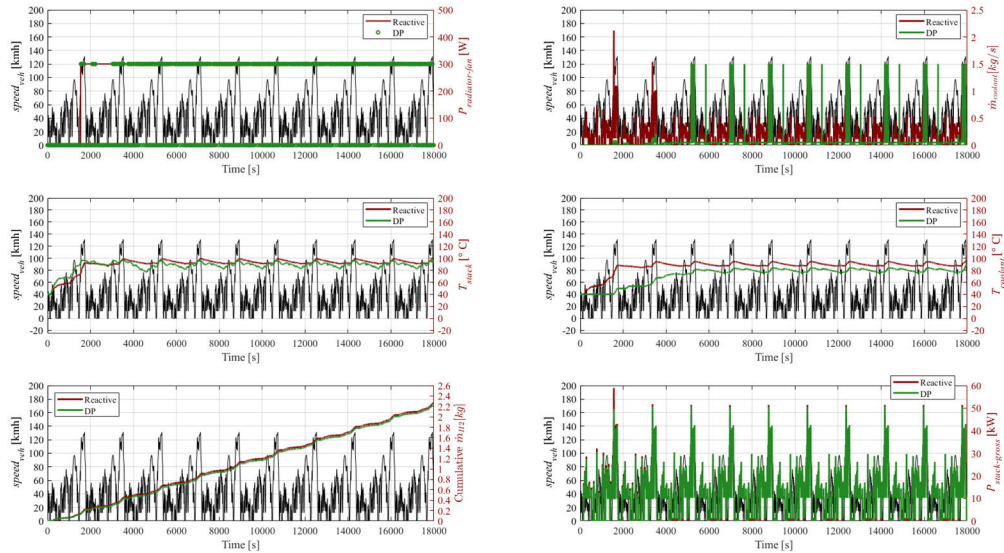
FIGURE 18. Time series of control and state variables for the FCEV simulated at 40 °C ambient temperature being controlled by both DP and the baseline reactive control strategy from Advisor in WLTCx10.

TABLE 6. Energy statistics for the fuel cell system simulated being controlled by DP and by the baseline reactive control strategy from Advisor over different numbers of WLTC repetitions at 40 °C ambient temperature.

		WLTCx1		WLTCx3		WLTCx10	
		Advisor	DP	Advisor	DP	Advisor	DP
Energy loss [kJ]	Air compressor energy	1659	1516	4765	4577	15609	15363
	Coolant pump energy	616	134	1839	1045	6116	6755
	Radiator energy	77	30	1157	314	4939	2145
	Condenser fan energy	328	328	985	985	3282	3282
	Chemical loss	10387	9256	29106	27544	94248	92741
Statistics	Net energy generation [kJ]	14745	14745	44234	44234	147446	147446
	Gross energy generation [kJ]	17424	16753	52980	51155	177392	174991
	Average stack efficiency [%]	62.7	64.4	64.5	65.0	65.3	65.4
	Average FC system efficiency [%]	53.0	56.7	53.9	56.2	54.3	55.1
	H2 consumption [kg]	0.23	0.22	0.68	0.66	2.26	2.23
	Driving mission length [km]	23.4	23.4	70.2	70.2	234.0	234.0
	Predicted H2 economy [kg/100 km]	0.99	0.93	0.97	0.93	0.97	0.95

results have been presented for a case study regarding the optimal thermal management of fuel cell systems in FCEVs. Several DP simulations have been performed by sweeping the number of steady repetitions of WLTC and the value of ambient temperature.

In general, the presented methodology has identified a global optimal operation that significantly reduces both the operational times of radiator fan and coolant pump and the coolant mass flow rate delivered by the pump. When compared with the baseline reactive control technique, the best off-line benchmark can save up to 10.2% hydrogen in correspondence with a short journey in extreme low temperatures. When either the length of the trip or the ambient temperature increase, however, the hydrogen saving capacity compared

with the baseline reactive control strategy steadily declines. Low temperatures are the lone exception in this scenario since a medium distance trip is suggested entailing lower hydrogen saving capability than a long distance trip. As concerns the different test cases, the optimal thermal control benchmark found by DP involves incrementally reducing the operational time and the auxiliary power consumption of the coolant pump. For this reason, the average fuel cell stack temperature increases and the overall fuel cell system efficiency consequently improves by some percentage points. Moreover, the optimal thermal management predicts lower uses of the radiator fan and coolant pump as hydrogen saving enablers especially for long distance trips. Moreover, significant energy and hydrogen savings are predicted to be

achieved by activating the radiator fan only at high values of vehicle speed, as in highway driving.

A. FUTURE WORK

Regarding related future work in this area, the fidelity of the modelling approach for both fuel cell system and vehicle could be refined and updated to the most recent technology. Moreover, the limitations of the proposed optimal control approach could be addressed towards developing on-board real-time predictive thermal management systems for FCEVs. Removing the a priori knowledge requirement for the driving mission and reducing the computational const are namely the two main restraints for on-board real-time implementation. Two examples of methods for enabling real-time predictive thermal management of FCEVs based on the present study involve heuristic and deep learning approaches. Concerning heuristic controllers, the presented results could be used as reference to extract control rules that real-time regulate the coolant mass flow rate in the pump and the radiator fan state. As a further option, a physics-informed deep learning framework could be developed for thermal management of FCEVs, where the physics-based domain knowledge provided off-line by DP is fed into the data-driven model as soft constraints to adjust the data-driven model [43], [44].

Real-time predictive thermal management could be an important feature to be integrated in recently developed energy management approaches towards real-world hydrogen saving in FCEVs [45], [46], [47], [48], [49]. Then, real-time control strategy for thermal management for FCEVs could be tested performing both Processor-In-the-Loop (PIL) and, Hardware-In-the-Loop (HIL) tests. The provided DP off-line approach may be used to generate the ideal benchmark and off-line optimized training data in this context.

APPENDIX

A.1 SIMULATION RESULTS FOR COLD TEMPERATURES
See Figures 10–12 and Table 4.

A.2 SIMULATION RESULTS FOR MILD TEMPERATURES
See Figures 13–15 and Table 5.

A.3 SIMULATION RESULTS FOR HOT TEMPERATURES
See Figures 16–18 and Table 6.

REFERENCES

[1] A. Ajanovic and R. Haas, "Economic and environmental prospects for battery Electric- and fuel cell vehicles: A review," *Fuel Cells*, vol. 19, no. 5, pp. 515–529, Oct. 2019.

[2] A. G. Boulanger, A. C. Chu, S. Maxx, and D. L. Waltz, "Vehicle electrification: Status and issues," *Proc. IEEE*, vol. 99, no. 6, pp. 1116–1138, Jun. 2011.

[3] R. Xiong, S. M. Sharkh, H. Li, H. Bai, W. Shen, P. Bai, and X. Zhou, "IEEE access special section editorial: Advanced energy storage technologies and their applications," *IEEE Access*, vol. 8, pp. 218685–218693, 2020.

[4] O. Bethoux, "Hydrogen fuel cell road vehicles: State of the art and perspectives," *Energies*, vol. 13, no. 21, p. 5843, Nov. 2020.

[5] X. Gong, F. Dong, M. A. Mohamed, O. M. Abdalla, and Z. M. Ali, "A secured energy management architecture for smart hybrid microgrids considering PEM-fuel cell and electric vehicles," *IEEE Access*, vol. 8, pp. 47807–47823, 2020.

[6] M. Carignano, V. Roda, R. Costa-Castelló, L. Valiño, A. Lozano, and F. Barreras, "Assessment of energy management in a fuel cell/battery hybrid vehicle," *IEEE Access*, vol. 7, pp. 16110–16122, 2019.

[7] X. Lin and J. Huang, "Applications of heuristic dynamic programming in the proton exchange membrane fuel cell temperature control," in *Proc. Power Eng. Autom. Conf.*, Wuhan, China, Sep. 2012, pp. 1–4.

[8] W.-J. Zou and Y.-B. Kim, "Temperature control for a 5 kW water-cooled PEM fuel cell system for a household application," *IEEE Access*, vol. 7, pp. 144826–144835, 2019.

[9] Y. Tian, Q. Zou, and Z. Lin, "Hydrogen leakage diagnosis for proton exchange membrane fuel cell systems: Methods and suggestions on its application in fuel cell vehicles," *IEEE Access*, vol. 8, pp. 224895–224910, 2020.

[10] S. Petrovic and E. Hossain, "Development of a novel technological readiness assessment tool for fuel cell technology," *IEEE Access*, vol. 8, pp. 132237–132252, 2020.

[11] S. Rashidi, N. Karimi, B. Sunden, K. C. Kim, A. G. Olabi, and O. Mahian, "Progress and challenges on the thermal management of electrochemical energy conversion and storage technologies: Fuel cells, electrolysers, and supercapacitors," *Prog. Energy Combustion Sci.*, vol. 88, Jan. 2022, Art. no. 100966.

[12] P. B. Gowda, S. C. Murthy, and R. Chandrashekar, "Research needed for proton exchange membrane fuel cell to enable automotive applications," in *Proc. Int. Conf. Innov. Mech. Ind. Appl. (ICIMIA)*, Bangalore, Feb. 2017, pp. 423–426.

[13] Q. Chen, G. Zhang, X. Zhang, C. Sun, K. Jiao, and Y. Wang, "Thermal management of polymer electrolyte membrane fuel cells: A review of cooling methods, material properties, and durability," *Appl. Energy*, vol. 286, Mar. 2021, Art. no. 116496.

[14] C. Lyu and V. R. Dinavahi, "Supervisory real-time multidomain modeling and hardware emulation of fuel-cell hybrid electric bus behavioral transients," *IEEE Access*, vol. 10, pp. 85975–85985, 2022.

[15] B. M. Kim and S. J. Yoo, "Approximation-based adaptive control of constrained uncertain thermal management systems with nonlinear coolant circuit dynamics of PEMFCs," *IEEE Access*, vol. 8, pp. 83483–83494, 2020.

[16] N. Sulaiman, M. A. Hannan, A. Mohamed, P. J. Ker, E. H. Majlan, and W. R. Wan Daud, "Optimization of energy management system for fuel-cell hybrid electric vehicles: Issues and recommendations," *Appl. Energy*, vol. 228, pp. 2061–2079, Oct. 2018.

[17] J. Liu, H. Zhou, X. Zhou, Y. Cao, and H. Zhao, "Automative air conditioning system control—A survey," in *Proc. Int. Conf. Electron. Mech. Eng. Inf. Technol.*, Aug. 2011, pp. 3408–3412.

[18] G. Şefkat and M. A. Özel, "Experimental and numerical study of energy and thermal management system for a hydrogen fuel cell-battery hybrid electric vehicle," *Energy*, vol. 238, Jan. 2022, Art. no. 121794.

[19] J. Xu, C. Zhang, R. Fan, H. Bao, Y. Wang, S. Huang, C. S. Chin, and C. Li, "Modelling and control of vehicle integrated thermal management system of PEM fuel cell vehicle," *Energy*, vol. 199, May 2020, Art. no. 117495.

[20] B. S. K. K. Ibrahim, M. A. N. Aziah, S. Ahmad, R. Akmeliawati, H. M. I. Nizam, A. G. A. Muthalif, S. F. Toha, and M. K. Hassan, "Fuzzy-based temperature and humidity control for HV AC of electric vehicle," *Proc. Eng.*, vol. 41, pp. 904–910, Jan. 2012.

[21] W. Binrui, J. Yinglian, X. Hong, and W. Ling, "Temperature control of PEM fuel cell stack application on robot using fuzzy incremental PID," in *Proc. Chin. Control Decis. Conf.*, Jun. 2009, pp. 3293–3297.

[22] Y. Xie, Z. Liu, J. Liu, K. Li, Y. Zhang, C. Wu, P. Wang, and X. Wang, "A self-learning intelligent passenger vehicle comfort cooling system control strategy," *Appl. Thermal Eng.*, vol. 166, Feb. 2020, Art. no. 114646.

[23] J. Han, S. Yu, and S. Yi, "Advanced thermal management of automotive fuel cells using a model reference adaptive control algorithm," *Int. J. Hydrog. Energy*, vol. 42, no. 7, pp. 4328–4341, Feb. 2017, doi: 10.1016/j.ijhydene.2016.10.134.

[24] Z. Sun, Z. Chen, Y. Wang, and H. Yuan, "PEM fuel cell thermal management strategy based on multi-model predictive control," in *Proc. IEEE/IAS Ind. Commercial Power Syst. Asia (I&CPS Asia)*, Shanghai, China, Jul. 2022, pp. 625–630.

[25] X. Piao, X. Wang, and K. Han, "Hierarchical model predictive control for optimization of vehicle speed and battery thermal using vehicle connectivity," *IEEE Access*, vol. 9, pp. 141378–141388, 2021.

[26] B. Zhang, F. Lin, C. Zhang, R. Liao, and Y.-X. Wang, "Design and implementation of model predictive control for an open-cathode fuel cell thermal management system," *Renew. Energy*, vol. 154, pp. 1014–1024, Jul. 2020, doi: 10.1016/j.renene.2020.03.073.

[27] J. D. Rojas, C. Ocampo-Martinez, and C. Kunusch, "Thermal modelling approach and model predictive control of a water-cooled PEM fuel cell system," in *Proc. 39th Annu. Conf. IEEE Ind. Electron. Soc. (IECON)*, Vienna, Austria, Nov. 2013, pp. 3806–3811.

[28] S. Quan, Y.-X. Wang, X. Xiao, H. He, and F. Sun, "Feedback linearization-based MIMO model predictive control with defined pseudo-reference for hydrogen regulation of automotive fuel cells," *Appl. Energy*, vol. 293, Jul. 2021, Art. no. 116919.

[29] P. G. Anselma, S. Luciani, and A. Tonoli, "Making the case for predictive thermal management of fuel cell systems for electrified vehicles," in *Proc. IEEE Transp. Electrific. Conf. Expo (ITEC)*, Anaheim, CA, USA, Jun. 2022, pp. 255–260.

[30] P. G. Anselma, S. Luciani, and A. Tonoli, "Predictive control framework for thermal management of automotive fuel cell systems at high ambient temperatures," *IFAC-PapersOnLine*, vol. 55, no. 24, pp. 298–303, 2022.

[31] S. D. Gurski, "Cold-start effects on performance and efficiency for vehicle fuel cell systems," Ph.D. thesis, Virginia Tech, 2002.

[32] T. Markel, A. Brooker, T. Hendricks, V. Johnson, K. Kelly, B. Kramer, M. O'Keefe, S. Sprik, and K. Wipke, "ADVISOR: A systems analysis tool for advanced vehicle modeling," *J. Power Sources*, vol. 110, no. 2, pp. 255–266, Aug. 2002.

[33] J. Larminie and A. Dicks, *Fuel Cell Systems Explained*, 2nd ed. Chichester, U.K.: Wiley, 2003.

[34] D. G. Kroger, "Radiator Characterization and Optimization," Warrendale, PA, USA, SAE Tech. Paper 840380, Feb. 1984.

[35] C. M. Martinez, X. Hu, D. Cao, E. Velenis, B. Gao, and M. Wellers, "Energy management in plug-in hybrid electric vehicles: Recent progress and a connected vehicles perspective," *IEEE Trans. Veh. Technol.*, vol. 66, no. 6, pp. 4534–4549, Jun. 2017.

[36] Z. Chen, N. Guo, Q. Zhang, J. Shen, and R. Xiao, "An optimized rule based energy management strategy for a fuel cell/battery vehicle," in *Proc. IEEE Vehicle Power Propuls. Conf. (VPPC)*, Belfort, France, Dec. 2017, pp. 1–6.

[37] J. Shen and A. Khaligh, "A supervisory energy management control strategy in a battery/ultracapacitor hybrid energy storage system," *IEEE Trans. Transport. Electrific.*, vol. 1, no. 3, pp. 223–231, Oct. 2015.

[38] Y. Hui-ce, Z. Chong, G. Xun, H. Yun-feng, and C. Hong, "Energy management strategy of fuel cell hybrid electric vehicle based on dynamic programming," in *Proc. Chin. Autom. Congr. (CAC)*, Nov. 2020, pp. 3134–3139.

[39] C. Romaus, K. Gathmann, and J. Bocker, "Optimal energy management for a hybrid energy storage system for electric vehicles based on stochastic dynamic programming," in *Proc. IEEE Vehicle Power Propuls. Conf.*, Lille, France, Sep. 2010, pp. 1–6.

[40] X. Gong, H. Wang, M. R. Amini, I. Kolmanovsky, and J. Sun, "Integrated optimization of power split, engine thermal management, and cabin heating for hybrid electric vehicles," in *Proc. IEEE Conf. Control Technol. Appl. (CCTA)*, Hong Kong, Aug. 2019, pp. 567–572.

[41] H. Lee, C. Song, N. Kim, and S. W. Cha, "Comparative analysis of energy management strategies for HEV: Dynamic programming and reinforcement learning," *IEEE Access*, vol. 8, pp. 67112–67123, 2020.

[42] F. Miretti, D. Misul, and E. Spessa, "DynaProg: Deterministic dynamic programming solver for finite horizon multi-stage decision problems," *SoftwareX*, vol. 14, Jun. 2021, Art. no. 100690.

[43] J. Zhang, Y. Zhao, F. Shone, Z. Li, A. F. Frangi, S. Q. Xie, and Z.-Q. Zhang, "Physics-informed deep learning for musculoskeletal modeling: Predicting muscle forces and joint kinematics from surface EMG," *IEEE Trans. Neural Syst. Rehabil. Eng.*, vol. 31, pp. 484–493, 2023.

[44] J. Zhang, Y. Li, W. Xiao, and Z. Zhang, "Non-iterative and fast deep learning: Multilayer extreme learning machines," *J. Franklin Inst.*, vol. 357, no. 13, pp. 8925–8955, 2020.

[45] X. Meng, Q. Li, G. Zhang, T. Wang, W. Chen, and T. Cao, "A dual-mode energy management strategy considering fuel cell degradation for energy consumption and fuel cell efficiency comprehensive optimization of hybrid vehicle," *IEEE Access*, vol. 7, pp. 134475–134487, 2019.

[46] H. Lee and S. W. Cha, "Energy management strategy of fuel cell electric vehicles using model-based reinforcement learning with data-driven model update," *IEEE Access*, vol. 9, pp. 59244–59254, 2021.

[47] H.-B. Yuan, W.-J. Zou, S. Jung, and Y.-B. Kim, "A real-time rule-based energy management strategy with multi-objective optimization for a fuel cell hybrid electric vehicle," *IEEE Access*, vol. 10, pp. 102618–102628, 2022.

[48] M. Salem, M. Elnaggar, M. S. Saad, and H. A. A. Fattah, "Energy management system for fuel cell-battery vehicles using multi objective online optimization," *IEEE Access*, vol. 10, pp. 40629–40641, 2022.

[49] U. Javaid, A. Mehmood, A. Arshad, F. Imtiaz, and J. Iqbal, "Operational efficiency improvement of PEM fuel cell—A sliding mode based modern control approach," *IEEE Access*, vol. 8, pp. 95823–95831, 2020.

PIER GIUSEPPE ANSELMA (Member, IEEE) received the M.S. and Ph.D. degrees (Hons.) in mechanical engineering from Politecnico di Torino, Turin, Italy, in 2017 and 2021, respectively. In 2016 and 2019, he was a Master's Student Researcher and a Visiting Ph.D. Student Researcher with the McMaster Automotive Resource Centre (MARC), McMaster University, Hamilton, ON, Canada. He is currently a Postdoctoral Research Fellow with Politecnico di Torino.

He is the author or coauthor of more than 60 peer-reviewed international conferences and journal publications. He holds one patent. His research interests include the design of propulsion and brake systems and the development of smart energy management strategies related to electrified and automated road vehicles. He received three awards for his research, including the First Prize at the TRA Visions 2020 Young Researcher Competition, the Siebel Scholar, Class of 2021, and the IEEE Italy Section ABB 2022 Ph.D. Thesis Award.

SARA LUCIANI (Member, IEEE) received the M.S. degree in mechatronic engineering from Politecnico di Torino, Turin, Italy, in 2019. She is currently pursuing the Ph.D. degree in mechanical engineering. In 2020, she was a Visiting Ph.D. Student Researcher with Lehrstuhl für Fahrzeugtechnik (FTM), Technische Universität München, München, Germany. She is the author or coauthor of more than ten peer-reviewed international conferences and journal publications. She holds one patent. Her research interests include the design of battery states estimation algorithms based on data-driven approaches and the development of energy management strategies for fuel-cell electric vehicles.

ANDREA TONOLI received the Ph.D. degree in machine design from Politecnico di Torino, Turin, Italy, in 1993. He was a Faculty Member with Politecnico di Torino, in 1994. He was the Director of the Mechatronics Laboratory, Politecnico di Torino, from 2007 to 2011. He is currently a Full Professor with the Department of Mechanical and Aerospace Engineering, Politecnico di Torino. His research interests include the analysis, design, and control of electromechanical systems, with an emphasis on rotating machinery, active and passive magnetic bearings and dampers, piezoelectric transducers for vibration and motion control, and electromechanical systems for automotive applications.

• • •